Theory of Brønsted Acidity in Zeolites

J.C. Jansen, M. Stöcker, H.G. Karge and J. Weitkamp (Eds.)
Advanced Zeolite Science and Applications
Studies in Surface Science and Catalysis, Vol. 85

Theory of Brønsted Acidity in Zeolites

R.A. van Santen

Schuit Institute of Catalysis, Eindhoven University of Technology,
P.O. Box 513, 5600 MB Eindhoven, The Netherlands.

1. ABSTRACT

The nature of the chemical bond of protons in a zeolite is analysed on the basis of theoretical and spectroscopic results. Of interest is the dependence on zeolite structure as well as composition. The zeolitic OH bond is mainly covalent. Proton attachment to the zeolite lattice causes a weakening of neighbouring Si-O and Al-O bonds. The effective increase in volume of the bridging oxygen atom causes a local deformation, that changes the strength of the lattice-chemical bonds over a few bond distances. Proton concentration effects as well as lattice-composition effects can be understood on the basis of the lattice-relaxation model. The energetics of proton transfer is controlled by the need to stabilize the resulting Zwitter-ion. The positive charge on the cation becomes stabilized by contact with basic lattice-oxygen atoms.

2. Introduction

How the reactivity of the acidic protons attached to the framework-oxygen atoms in the micropores of zeolites depends on composition, location and zeolite framework is of obvious importance to the application of zeolites in acid catalyzed reactions. Whereas significant progress has been made to determine this relationship, it is still not completely understood. One of the reasons is the complexity of the catalytic reaction cycle, that is composed of different reaction steps. Proton transfer between lattice and substrate is only one of them and not necessarily always the rate limiting step. Secondly the acidity of the proton, as probed in the catalytic event depends on its state before reaction as well as the stability of the "Zwitter-ion" state, generated upon proton transfer to the reacting molecule. The latter may vary dependent on substrate and, as we will see, depends also strongly on the interaction between ion and zeolite wall.

Here we will discuss recent results of theoretical as well as spectroscopic studies probing the details of the chemical bond of the proton with the zeolite and the response of the proton with reacting basic molecules.

Protons in zeolites have been extensively studied using many different physical tech-

niques, especially infrared spectroscopy, NMR spectroscopy and neutron scattering. Because of their well-defined nature zeolites belong to the exceptional class of catalysts that allow for a definitive structural characterization of its catalytically active site. Computational chemical techniques require such detailed knowledge. The use of ab-initio calculations has contributed in an essential way to an understanding of the chemical features that control zeolite acidity. An important theoretical question we will address is the validity of the cluster approach to approximate the protonic site. A second important theoretical approach is the use of lattice-energy calculations and lattice-structure simulations based on force fields determined from accurate quantum-chemical calculations.

In the following two sections we will highlight our present understanding of the nature of the chemical bond of the proton. In a subsequent section we will present the results of theoretical studies on proton transfer to adsorbed basic molecules. It will appear that two properties of the solid state are very important to zeolite acidity:

- electrostatics, the positive charge developing on the proton has to be compensated by a negative charge generating on the zeolite lattice.
- lattice relaxation, changes in chemical bonding affect the forces acting on the lattice atoms involved.

In a final section the implications of the physical chemistry of proton transfer to acid catalysis will be shortly outlined.

3. The proton Bond

The zeolite lattice consists of a three dimensional network of tetrahedra connecting four valent or three valent metal cations such as Si or Al, each having four oxygen atoms as neighbours. One oxygen atom has two metal cations as nearest neighbours (figure 1). When all lattice ions are Si, the zeolite lattice has the composition SiO_2 and is a polymorph of quartz. Brønsted acidic sites are generated when silicon, which has a formal valency of four, is replaced by a metal atom with a lower valency. Most common is the replacement of silicon by aluminum with a formal valence of three. A proton is attached to the oxygen atom connecting a neighbouring silicon and aluminum atom, resulting in a chemically stable situation. Note that now the oxygen atom becomes three coordinated.

Quantum-chemical calculations have convincingly shown that the SiO, AlO as well as the OH bonds have considerable covalency, resulting in a relatively weak OH bond. The "onium" type coordination of oxygen is the fundamental reason for the high acidity of the attached proton. Cluster calculations on H or OH terminated rings in figure 2 give illustrations of such geometries providing detailed geometric information on the acidic site [1]. The results of ab-initio cluster calculations on protonated rings formed from four tetrahedra are shown. As we will see crystallographically different sites in a zeolite show small differences. One of the most interesting features is the long Al-O bond compared to the Si-O bond (0.188 nm and 0.172 nm respectively). The acidic site can also be seen as a silanol group promoted by a the Lewis acidic group. Whereas the OH bondlength changes little, the heterolytic bond energy changes from approximately 21.8 eV [2] to 13.7 eV [3].

Kazansky [4] has analyzed the OH interaction-potential by an analysis of the overtones of the OH stretch frequencies measured in the near infrared spectroscopic range.

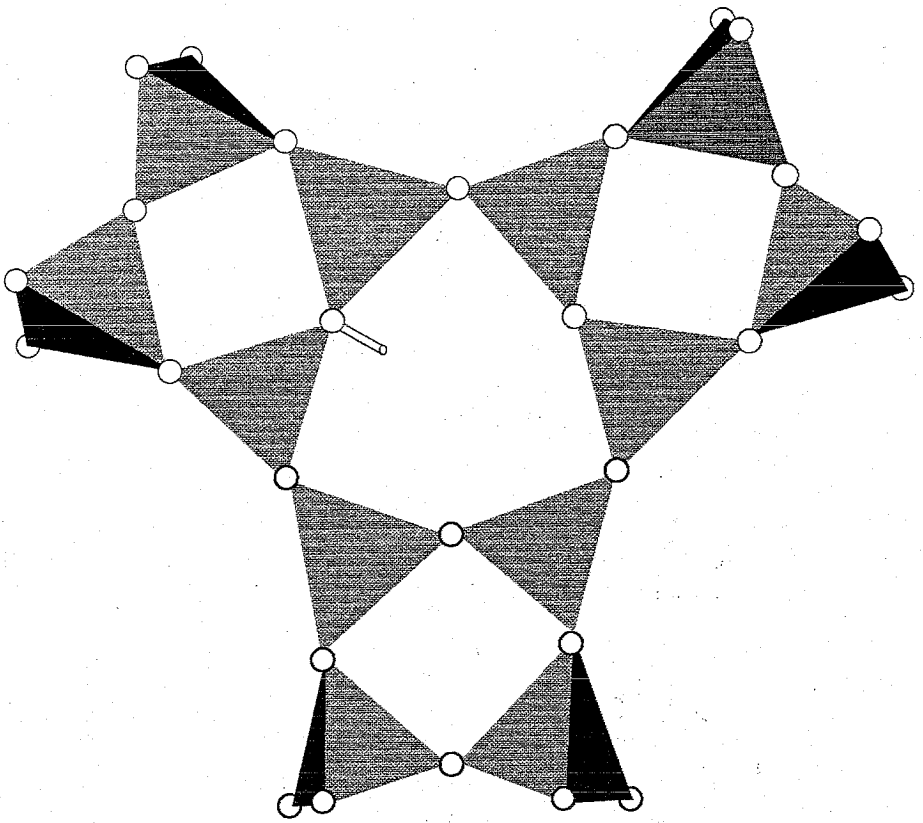

Figure 1. Connectivity of T-atoms. The T-atoms are in the centre of the tetrahedra formed by four oxygen atoms: when one silicon atom is replaced by an aluminum atom and a neighbouring oxygen atom becomes protonated.

He found that the covalent OH interaction-energy varies little with acidity. The constant homolytic bondstrength of OH indicates that the factor that contributes most to the strong acidity is mainly the increased stabilization of the negative charge left on the lattice with deprotonation.

1H MAS NMR spectra enable the experimental determination of the Al-H distance [5]. For zeolite Y values of 0.237 nm and 0.248 nm have been found for protons located in the supercages and sodalite cages respectively.

The cluster calculations indicate a large change in the equilibrium geometry of the ditetrahedral cluster upon deprotonation (compare figures 2a and 2b, atom-position 8). As is shown in figure 2b, the AlO and SiO distances shorten. These changes are a consequence of covalent bonding and the Bond Order Conservation principle [6]. Since no electrons of the bridging oxygen atom are involved any more in bonding with the OH bond, they become available to additional bonding for AlO and SiO. The result is an increase in the SiO and AlO bondstrengths.

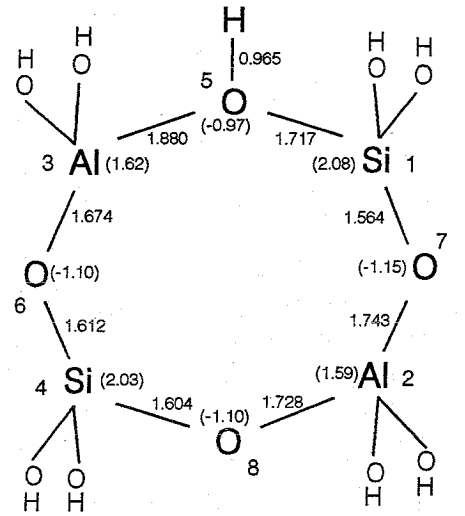

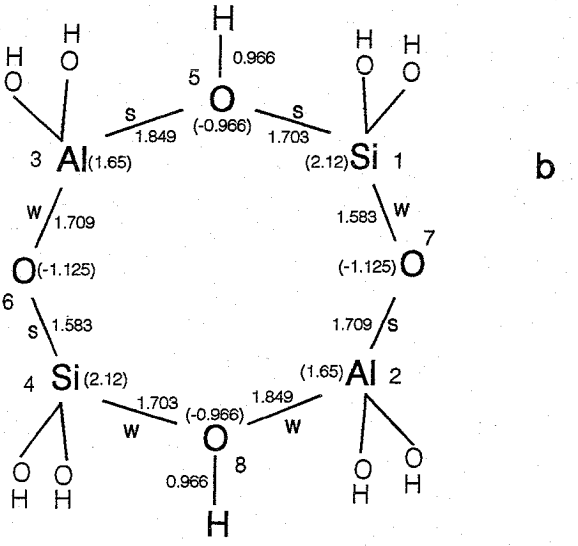

Figure 2. 165 Four-ring cluster containing two silicon and two aluminum atoms and one (a) or two (b) acidic protons [1].

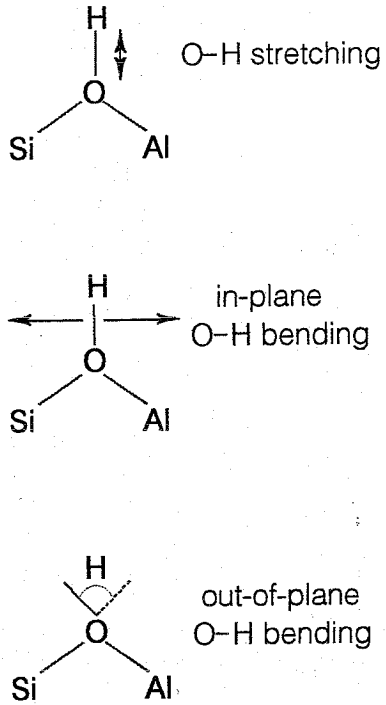

Figure 3. The three vibrational modes of the Brønsted acidic group.

Ab-initio quantum-chemical calculations also provide information on the vibrational modes of the OH group. Infrared spectroscopy and inelastic neutrons scattering [7] can be used to compare predictions with experiments. The three vibrational modes of the Brønsted acidic group are sketched in figure 3. Typical values of the OH stretch frequencies of the Brønsted acidic protons vary between 3650 and 3550 cm^{-1}, to be compared with the silanol frequency at 3745 cm^{-1}. The relatively small decrease in stretch frequency corresponds to a slightly weakened OH force constant of the acidic protons. The in plane bending mode of the Brønsted acidic protons has a frequency of approximately 1050 cm^{-1} [7-10], the out-of plane bending mode of approximately 400 cm^{-1} [7,9,10]. Indirect measurement of the bending modes are available from infrared combination bands [7,8]. Direct measurements have been done using inelastic neutron scattering spectroscopy [7,10]. Experimental and theoretical values [9] are in close agreement.

Experimental indications of local structural relaxation upon deprotonation have been provided by infrared spectroscopic studies of the lattice-modes of zeolite Y, comparing the spectra of NH_4-Y with the H-Y form [11]. Figure 4a shows the corresponding infrared

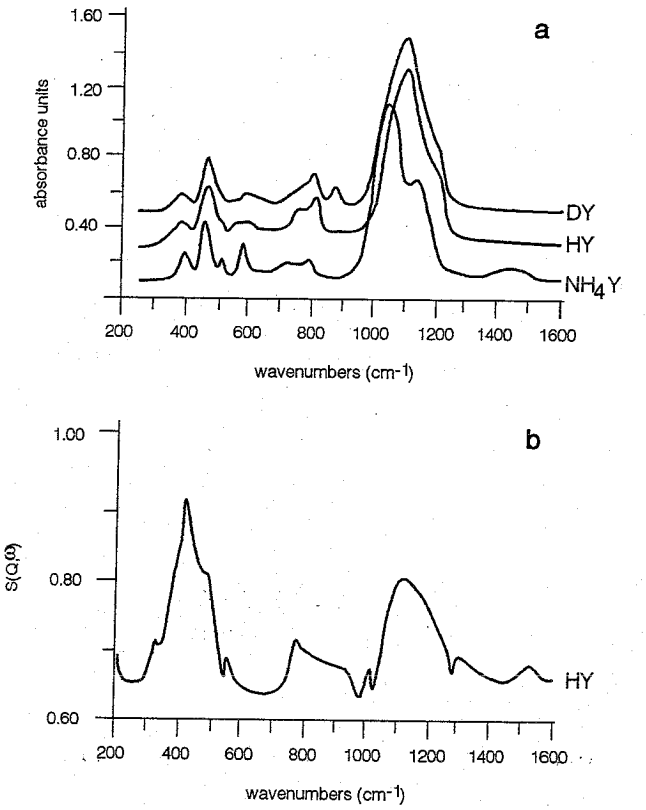

Figure 4. Infrared active lattice modes of NH_4Y, HY, DY (a) [11,12], and inelastic neutron scattering spectrum of HY (b) [7].

spectra. Also shown are the frequencies of the bending OH modes as measured by inelastic neutron scattering (figure 4b).

Protonation of the zeolite lattice results in significant changes of the lattice vibrational modes. One observes an upwards shift around 750 and 1100 cm^{-1}, decreases in intensity around 600 cm^{-1} and smaller changes at 400 cm^{-1}. Figure 4a shows also the infrared spectrum of deuterated zeolite Y. New peaks arise near 860 cm^{-1}[12]. The shifts around 750 and 1100 cm^{-1} and the losses in intensity below 600 cm^{-1} remain. Clearly in the region from 700 to 1100 cm^{-1} there is a strong coupling between the in-plane OH bending mode and the Si-O-Al stretching modes, that are resonant in energy. The existence of this coupling between the OH bending modes and the lattice modes is concluded from results from inelastic neutron scattering experiments [10]. Here, due to the coupling, the intensity of the lattice modes of H-Y zeolites is increased compared to those for Na-Y zeolites. The intensity of the modes between 600 - 300 cm^{-1} change very similarly for

the protonated as well as deuterated system. The modes are mainly combinations of tetrahedral bending modes as well as Si-O-Al symmetric stretching modes, sensitive to deformation of the lattice [13]. These changes are due to the deformation of the lattice upon protonation.

Whereas the results of the ab-initio cluster calculations indicate the possibility of structural deformation upon protonation, embedding of the cluster in the three dimensional zeolite lattice is needed in order to evaluate to which degree it actually will occur in the solid. This can be conveniently done using energy minimization schemes applicable to the solid state. The equilibrium atomic geometries can be computed using atomic force fields [14]. Such force fields can be developed based on a fit of the parameters of classical interatomic potentials to potential energy surfaces computed quantum-chemically for small clusters [15]. One concludes from such studies that the changes in local chemical bonding due to proton attachment also lead to deformation of the lattice. However, the deformations are very local and disappear at a few atomic distances from the proton location [16]. This is illustrated in figure 5 for proton attachment to the O(1) atom of the double-six ring of faujasite. The geometry optimized structures of the protonated and non-protonated sites are compared. Atom positions before and after proton attachment are shown. One observes the longer SiO and AlO distances of the protonated system and the rapid decline of the bondlength changes at a larger distance from the proton.

Sites generated upon protonation require more space than the proton-free site. In zeolites atom distances of the lattice atoms vary for crystallographically different positions. One may expect to find a relation between bond angles and bondlengths around a site before protonation and the protonation energy. Structural and compositional effects will be discussed in the next section. The main conclusion of this section is that experimentally as well as theoretically local structural relaxation can be considered well established.

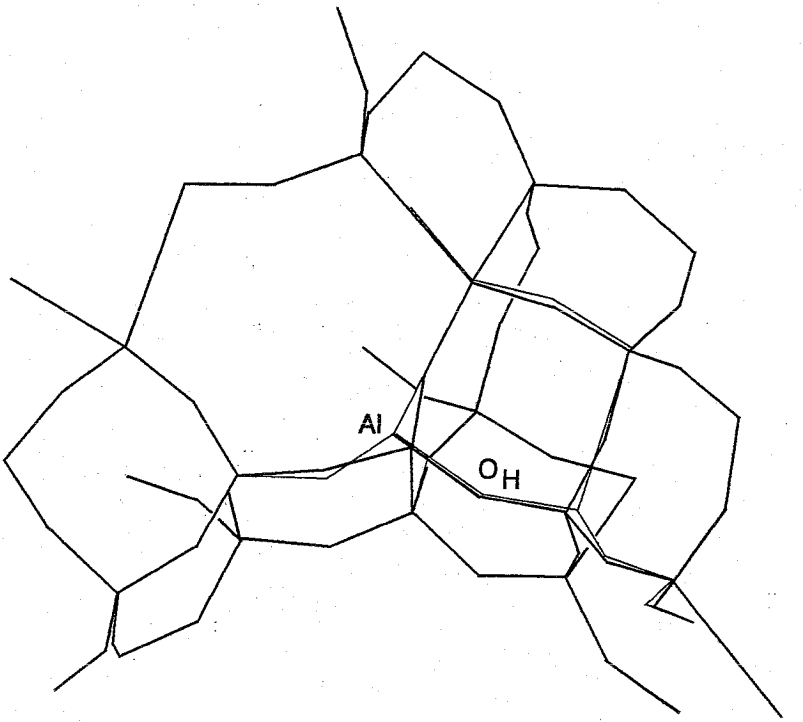

Figure 5. Lattice relaxation due to protonation of the double-six ring in the Faujasite lattice [16].

4. Proton affinity differences.

When one compares the stretch frequency of the OH bond in a zeolite in the same structure but varying the aluminum content, small changes in the infrared frequency are observed. Figure 6 shows the change in the infrared frequencies of high-frequency OH stretching modes in zeolite Y as a function of increasing Si/Al ratio [17]. Whereas at a ratio of Si/Al = 2.4, one observes only the silanol and two Brønsted acidic hydroxyl groups for zeolite Y (the high-frequency and low-frequency bands), upon an increase of the Si/Al ratio infrared HF OH peaks at lower frequencies appear, indicative of a stronger Brønsted acidity. This is in agreement with the shift to lower field of the corresponding lines in the 1H MAS NMR spectra (see figure 6).

In a zeolite according to the Löwenstein rule, aluminum ions cannot occupy neighbouring tetrahedra. This exclusion principle derives from the negative charge build up around the two tetrahedra leading to repulsive effects. At a low Si/Al ratio each [Si-O-Al] unit is connected to six tetrahedra of which a maximum of three is occupied by Al.

In the faujasite lattice positions are equivalent, but the four oxygen atoms forming a tetrahedron are non-equivalent (figure 7). Of these four oxygen atoms, protons are

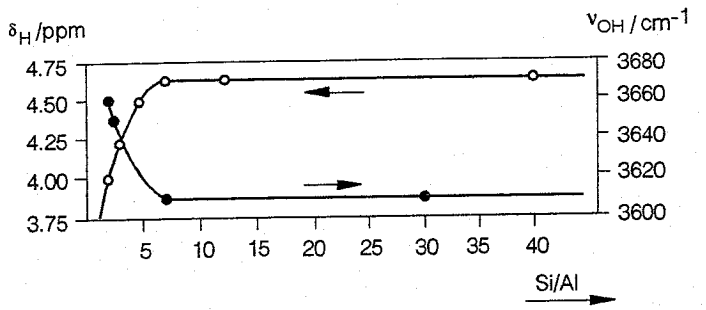

Figure 6. Infrared high-frequency OH stretch frequency (OH) as a function of the Si/Al ratio [17] and chemical shift (H) of the corresponding line in the 1H MAS NMR spectrum as a function of the Si/Al ratio.

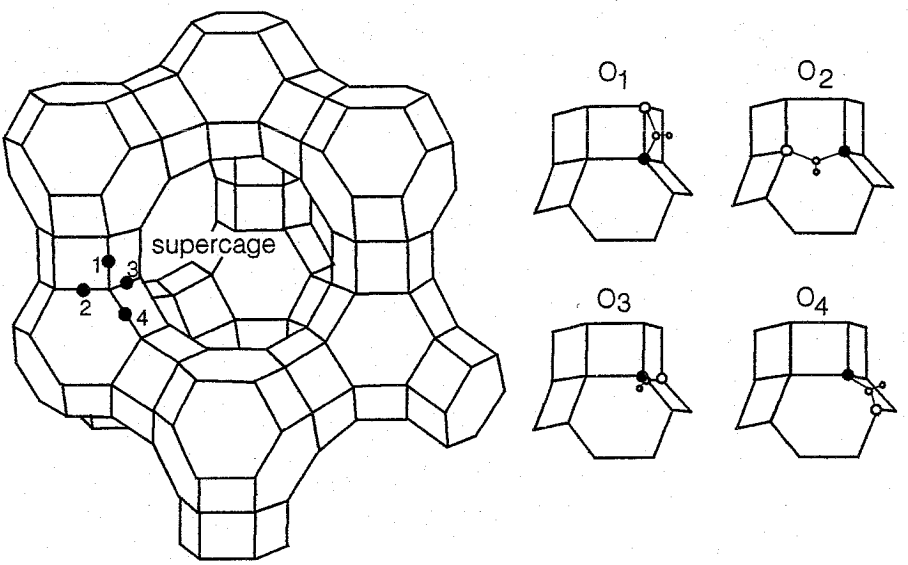

Figure 7. The four different oxygen atoms in the Faujasite lattice[21].

Table 1.
Total energies (in atomic units) and proton affinities (in eV) of 4-ring clusters. Complete geometry optimizations were performed at the STO-3G level; the 3-21G results refer to the STO3G-optimized geometry with an additional optimization of the proton position. Results marked by an asterisk refer to the abstraction of one proton only; the result in parentheses is influenced by a different configuration of the terminal hydrogen atoms [1]

		A:STO3G optimized geometry		B:3-21G STO3G geometry		C:3-21G optimized geometry	
	ring	E(a.u.)	PA(eV)	E(a.u.)	PA(eV)	E(a.u.)	PA(eV)
1	SiSiSiSi	-203.318558		-2048.522833			
2	$Si^{H}SiSiSi$	-203.779993	12.56	-2048.839850	8.63		
3	AlSiSiSi	-201.331399		-2001.777284		-2001.850643	
4	$Al^{H}SiSiSi$	-202.002739	18.27	-2002.279709	13.67	-2002.374317	14.25
5	$AlSi^{H}SiSi$	-201.925292	16.16	-2002.208117	11.72	-2002.309532	12.49
6	$Al^{H}SiSiSi^{H}$					-2002.749718	10.22*
7	AlSiAlSi					-2002.988098	
8	AlAlSiSi	-199.161940		-1954.885995			
9	$Al^{H}SiAlSi$	-200.024318	21.98	-1955.542784	16.77	-1955.626118	17.36
10	$Al^{H}Si^{H}AlSi$	-200.633693	16.58*	-1955.994844	12.29*	(-1956.120927	13.46*)
11	$Al^{H}SiAl^{H}Si$	-200.726481	19.10*	-1956.067643	14.27*	-1956.163893	14.63*
12	$AlSi^{H}Al^{H}Si$	-200.683936	17.94*	-1956.024463	13.11*	-1956.1256167	13.58*

attached most strongly to O(1) and O(3) sites, giving rise to a HF (3650-3610 cm^{-1}) and LF (3550-3570 cm^{-1}) OH infrared absorption peak. The reasons for this will be discussed below. With a decrease of aluminum content, the probability for a [Si-OH-Al] unit to be surrounded by three tetrahedra with aluminum decreases. With a statistical distribution of aluminum over the tetrahedra (constrained by Löwenstein's rule) now different embedding possibilities of the [Si-OH-Al] unit exist. The frequency changes for the HF OH depend only on changes of composition in tetrahedra in the first coordination shell of the [Si-OH-Al] unit and converge to the same value at Si/Al>>10.

A decreasing heterolytic proton bond dissociation energy with increasing Si/Al ratio is also found from ab-initio calculations on clusters of varying Si/Al content. Figure 8 shows rings of four tetrahedra, terminated by end-on OH groups with varying Si/Al ratio. As follows from the corresponding table 1 the deprotonation energy is smallest for the tetrahedral four ring with one aluminum atom and the protons prefer attachment to an oxygen atom also coordinated to an aluminum atom. When the aluminum content increases, the deprotonation energy increases for a cluster with 2 protons as well as the negatively charged cluster, simulating compensation by cations. In figure 2 the corresponding geometries and charges are shown.

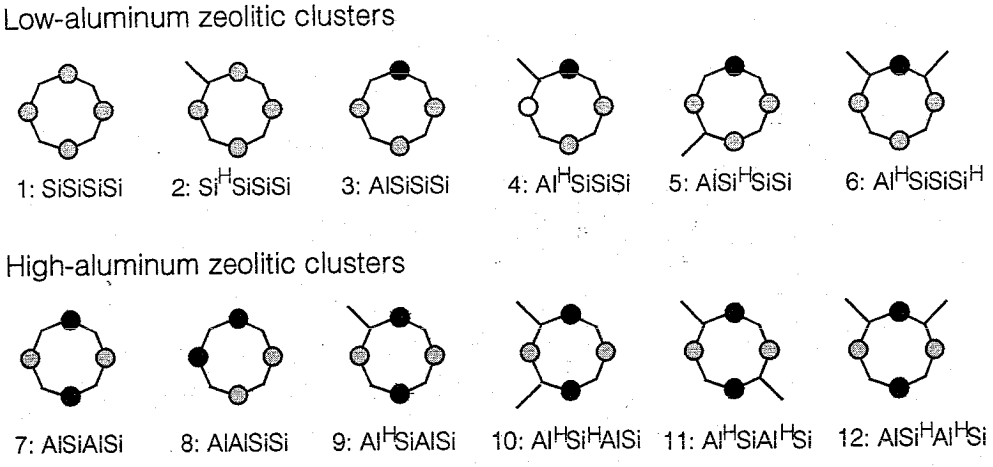

Figure 8. Four-ring clusters with different Si/Al ratios and different proton concentrations[1], see also table 1.

Experimentally the Brønsted acidity of zeolite Y appears to be a strong function of proton content. In figure 9 calorimetric measurements are presented of the ammonia adsorption on zeolite Y with three different compositions [18,19]. The interaction with zeolite Y (Si/Al = 2.4) is compared at 100% proton exchange and 85% proton exchange. One notes a significant increase in the initial heat of adsorption due to protonation of ammonia. The same increase in heat of adsorption is found for the dealuminated material.

Adding a proton to position O(8) results in a weakening of the O(5) - H bond, (enhancing the intrinsic Brønsted acid strength) and a strengthening of the neighbouring Si(3) - O(5) and Al(1) - O(5) bonds. This can be deduced from the bondlength differences in figure 2. Whereas proton attachment to position O(8) lengthens the Si(2) - O(8) and Al(4) - O(8) bonds, the next Si(2) - O(7) and Al(4) - O(6) bonds become stronger. As a function of distance to the proton on O(8) these changes alternate causing the O(5) - H bond to weaken. This again is a consequence of covalent bonding and the Bond Order Conservation principle. When one of the bonds to an atom weakens, the other will become stronger. The changes in atomic charges are very small hence one concludes that proton-strength differences are dominated by changes in covalent bondstrength.

For the LF OH peaks in zeolite Y a different behaviour upon dealumination is observed. With increasing Si/Al ratio the maximum for this band is shifted to higher frequencies. This behaviour cannot be explained by the small clusters discussed here, since the acidic protons, which are responsible for this infrared band, interact with two close oxygen neighbours at a distance of 0.26 nm [20].

To relate changes in OH bondstrength with composition to changes in lattice covalent bonding is one way of interpreting consequences of changes in electron density. As discussed elsewhere analysis in terms of HOMO-LUMO interactions leads to very similar conclusions [6]. It is important to realize that the changes in acidity are ascribed to electron-density differences and not to changes in atom charges.

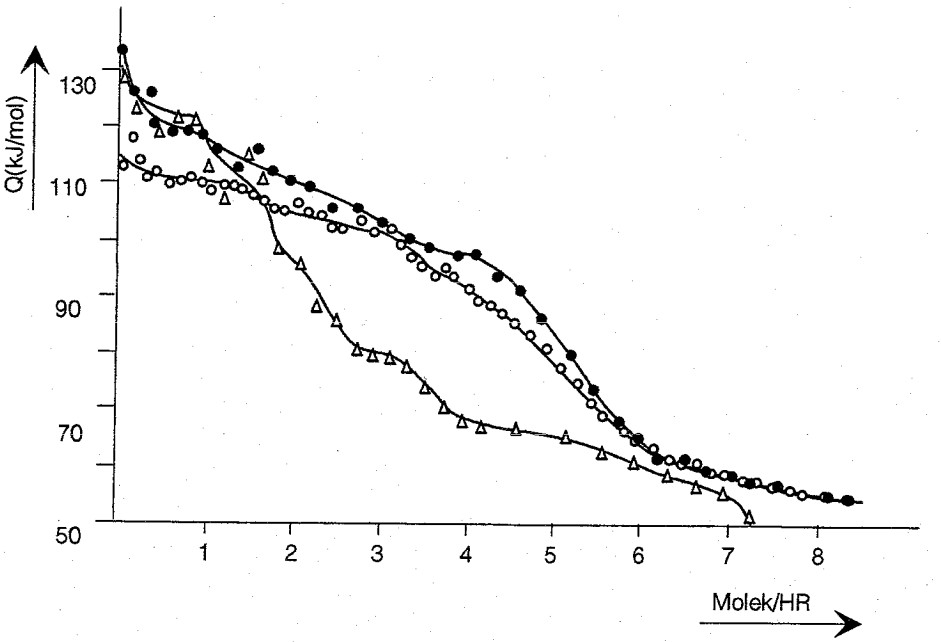

Figure 9. Differential heat of sorption (Q) versus the number of NH_3 molecules per supercage, measured at 423 K on Y type zeolites [19]: o NaY(85), Si/Al=2.4; • HY(100), Si/Al=2.4; Δ DY-3, Si/Al=4.1.

Using force-fields, differences in proton affinity have been theoretically analyzed for two low aluminum content zeolite frameworks: zeolite Y which is a low density zeolite and silicalite of high density [1,21]. In zeolite Y the four oxygen-atom positions are non-equivalent. In silicalite 12 atom-positions are non-equivalent and 48 different oxygen atom positions are in principle possible. The deprotonation energy is calculated for fully relaxed bridging oxygen sites in the presence and absence of an added proton. These studies have demonstrated the importance of the zeolite lattice structure for the intrinsic Brønsted acidity of lattice protons. It is found that the deprotonation energies vary within an interval of 20 kcal/mole for different sites. For the MFI structure the amount of structural relaxation and corresponding energy gain is found to vary very little for the different sites, whereas there are large differences for the protonation energies. The parameter of the fully relaxed SiO_2 polymorph that correlates strongly with the OH interaction strength at a particular site is the SiO bondlength (figure 10). The larger the average SiO bondlength the stronger the OH bond. This is in line with the previously discussed bulkiness of the [Si-OH-Al] group compared to the Si-O-Si unit. The strongest Brønsted acidic sites are found at sites that are spatially most constrained.

According to the results presented, the dominant effect controlling the OH bondstrength is the proton concentration (see table 1). When the proton concentration is low, the in-

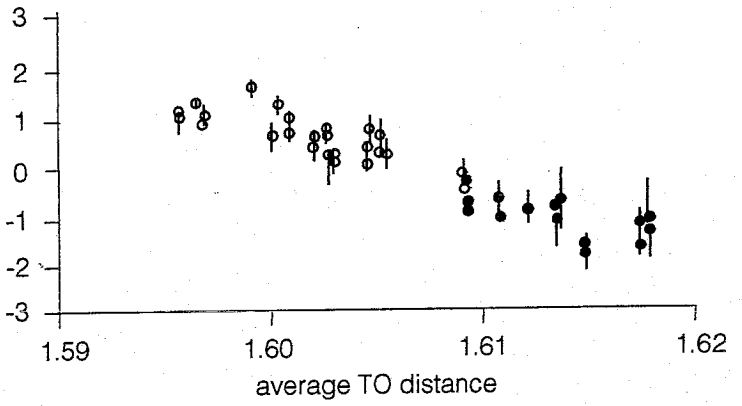

Figure 10. Relation between average T-O distance, O-O distance and T-O-T angle in the relaxed all-silica structure of MFI, and the (averaged) proton energy of the corresponding oxygen site [1].

trinsic Brønsted acidity per proton increases with decreasing Al-concentration. Structural diffences have a comparable effect as variation in Si/Al ratio.

5. Proton-weak base interaction

An easily accessible probe of the intrinsic acidity of the zeolitic proton is the change in the infrared adsorption spectrum, when the proton interacts with a weakly interacting base. This is illustrated in figure 11 that shows the difference spectrum of the undisturbed P-OH group of a CoAPO II zeolitic material and that interacting with basic CD_3CN. The OH peak is found to be shifted to approximately 3100 cm^{-1}[22]. The spectral adsorption is significantly broadened and increased in intensity. The lower peak maximum is due to the weakening of the OH bond by interaction with the nitrile group:

The lone pair on nitrogen pushes electron density away from the proton, this results in an increase of its positive charge. It is reflected in the high absorption intensity that is proportional to the square of the induced OH dipole moment. The broadening of the peak is characteristic of hydrogen bonding and stems from anharmonic coupling to the motion of the $N\equiv C\text{-}CD_3$ molecule against of the proton. The features around 2300 cm^{-1} are due to the perturbed CN group and indicate the presence of Lewis as well as Brønsted acid sites[23].
Whereas the interaction of acetonitrile weakens the OH stretching modes, it shifts the

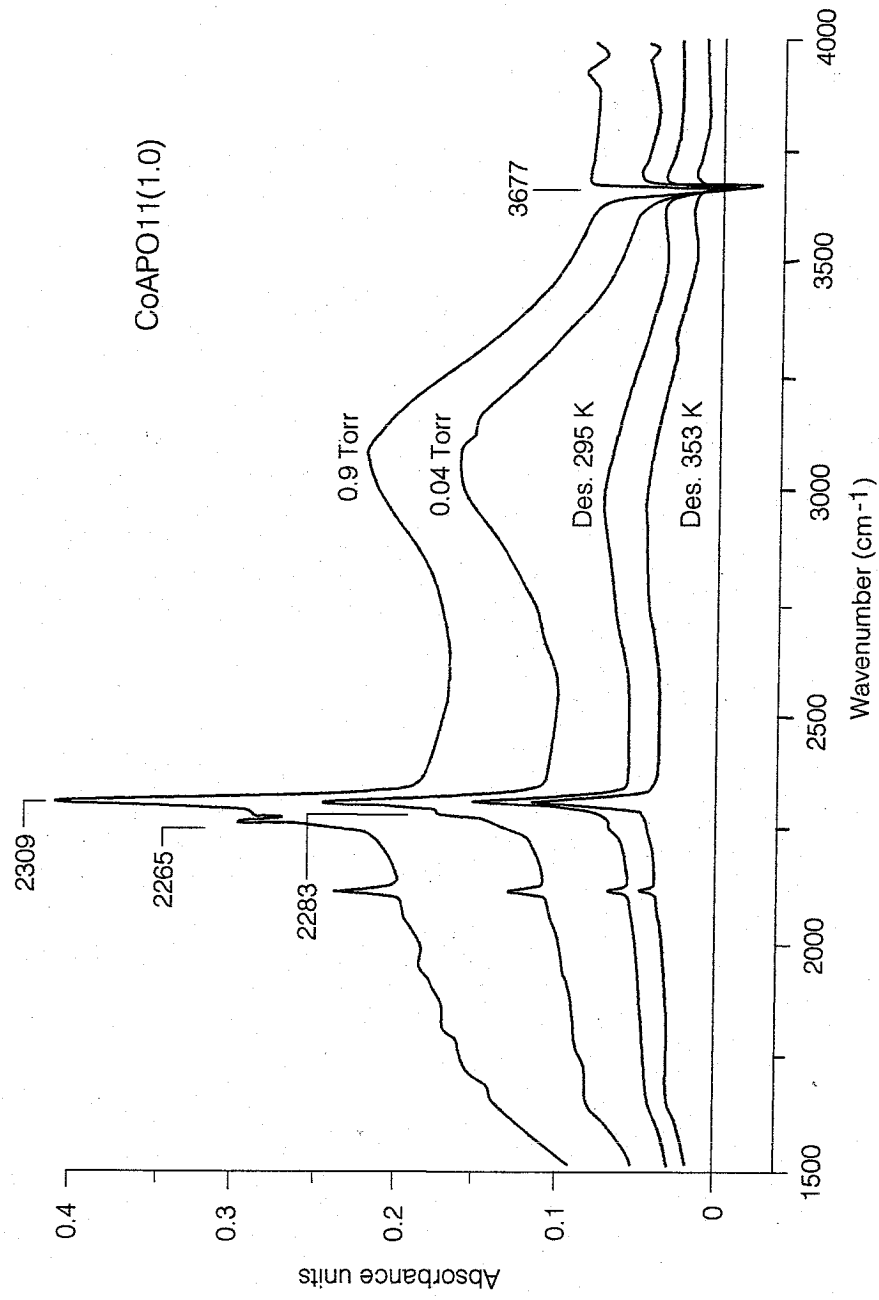

Figure 11. Difference Ft-IR spectra of CoAPO II by adsorption with CD_3CN.

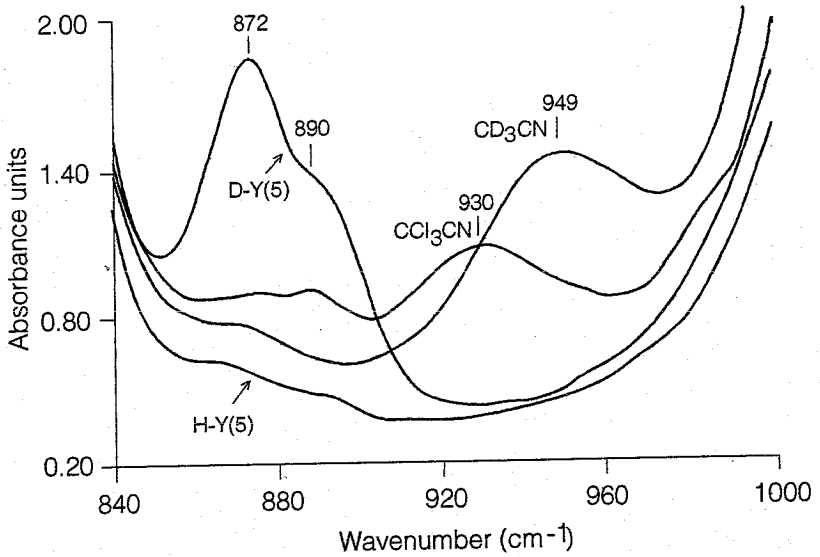

Figure 12a. Comparison of in-plane OD bending modes of DY (Si/Al=5) in the absence and presence of interacting CCl_3CN and CD_3CN.

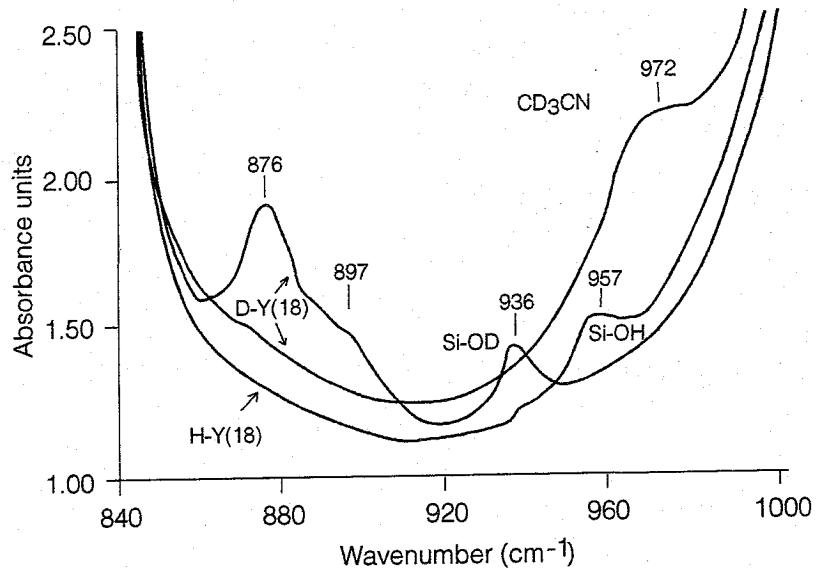

Figure 12b. In-plane OD bending modes of deuterated zeolite Y (Si/Al=18) in the absence and presence of CD_3CN. Also the spectrum of non-deuterated HY is shown.

frequency the OH bending modes upwards. This is due to the induced limited motion of the bending mode. Using deuterated zeolites, these upward shifts have been experimentally demonstrated[24]. In figures 12 the non-disturbed and disturbed OD bending modes of DY are shown. In the absence of base a weak shoulder is observed $\approx$25 cm^{-1} higher than the main peak at 872 cm^{-1}. The shoulder corresponds to the hydrogen bonded LF stretching peak (O(3)). Interaction with Cl_3CN gives a smaller upwards shift than CD_3CN. This is because Cl_3CN is a weaker base. The interaction with the basic adsorbates gives an upwards shift with 60-80 cm^{-1}. This is much more than the 25 cm^{-1} shift of the LF proton, due to interaction with other lattice oxygen atoms. Comparison of figures 12a and 12b illustrates the effect of the difference in intrinsic proton acidity. With a higher Si/Al ratio the proton is more weakly bonded and the upwards shift upon interaction with the basic molecule larger. The spectrum of the shifted zeolitic OH stretching frequency in contact with CD_3CN is more complex than that of the POH group. The spectra are shown in figure 13[23]. Instead of one single shifted peak as shown in figure 11, now a double peak appears in the spectrum. The average position of the shifted intensity, summed over the two peaks is approximately 2700 cm^{-1}. The stronger intrinsic acidity of the bridging OH group, compared to the POH group is the cause of the much larger shift of the bridging OH group. The double peak is due to large vibrational coupling effects that arise when the features of the shifted OH bond overlap with other protonic modes. Such a mode is the overtone of the upwards shifted in-plane OH bending modes. The corresponding fundamental frequency will have a value of approximately 1300 cm^{-1} and hence its overtone a frequency of 2600 cm^{-1}. The resulting Fermi resonance[23] causes the dip in the spectrum. It appears that the interaction with many basic molecules shows this doubly peaked structure in its spectrum. It can be considered a signature of hydrogen bonding in a zeolite. When H_2O or methanol interacts with protons the double peaked feature also appears, indicating that hydronium[25] or methoxonium[24] formation does not occur for these molecules in the ground state. In the next section we will discuss the proton-transfer reaction.

6. Proton-transfer

In the acid-base reaction:

$$ZH + B \rightleftharpoons Z^- + HB^+$$

charge is separated. In solution the cost of charge separation is overcome by solvation of the ions generated by solvent molecules. The dielectric constant of a zeolite is very small ($\sim$4), the energy of charge separation now has to be counteracted by the interaction between the positively charged protonated base and the negative charge of the zeolite wall.

Cluster-calculations on the protonation of NH_3 provide an interesting illustration of the importance of Zwitter-ion stabilization [26,27]. Very accurate ab-initio calculations of the NH_3-[Si-OH-Al] dimer interaction with the ammonia nitrogen atom coordinating to the bridging OH site show that the OH distance remains 0.098 nm to be compared with the long HN distance of 0.277 nm (figure 14a). So proton transfer does not occur. The

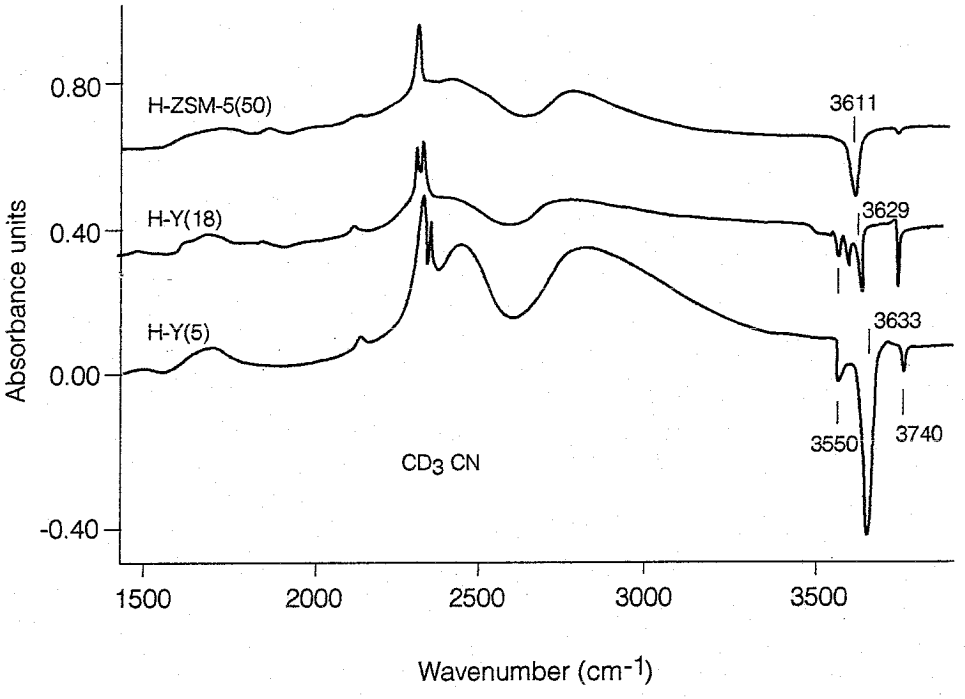

Figure 13. Difference spectra of H-ZSM-5 (Si/Al=50), H-Y (Si/Al=18) and H-Y (Si/Al=5) interacting with CD_3CN.

interaction between ammonia and OH shifts the OH frequency downwards by 380 cm^{-1} indicating a weakening of the OH bond. The computed interaction energy is 55 kJ/mole. The experimentally measured heat of adsorption of NH_3 is between 110 kJ/mole and 160 kJ/mole. Coordination as shown in figures 14b and 14c makes Zwitter-ion formation possible [27]. The NH_4^+ ion coordinates with two or three of its hydrogen atoms to the negatively charged oxygen atoms surrounding the Al atom. The computed interaction energies are very similar and equal to 114 kJ/mole. For the bidentate and tridentate bonded NH_4^+-ions, the infrared spectrum can be computed. Each coordination type is characterized by a different spectrum. Comparison with experimentally measured spectra enables an assignment of the two different coordination types (see table 2). Also the frequency of the external vibration of NH_4^+ versus zeolite wall can be computed. For the bidentate and tridentate bonded NH_4^+-ions the obtained frequencies vary from 250 to 350 cm^{-1} [28]. These low frequencies compare very well with typical values of NH_4^+ (80-200 cm^{-1}) found for zeolite Y [29]. The absence of hydrogen bonding is also evident from the non-appearance of the double-peaked infrared adsorption band around 2600 cm^{-1}.

Comparison of the geometry of the aluminum-tetrahedral cluster before NH_3 interaction (figure 13d) and the interacting clusters (figure 13b and 13c) show that the geometry around the tetrahedra changes when the proton is transferred. In a rigid lattice this would be prevented and as a consequence no proton transfer would occur. This is what is found theorically if no geometric relaxation is allowed when computing proton transfer. So proton-transfer requires a flexible lattice, that allows for local deformations.

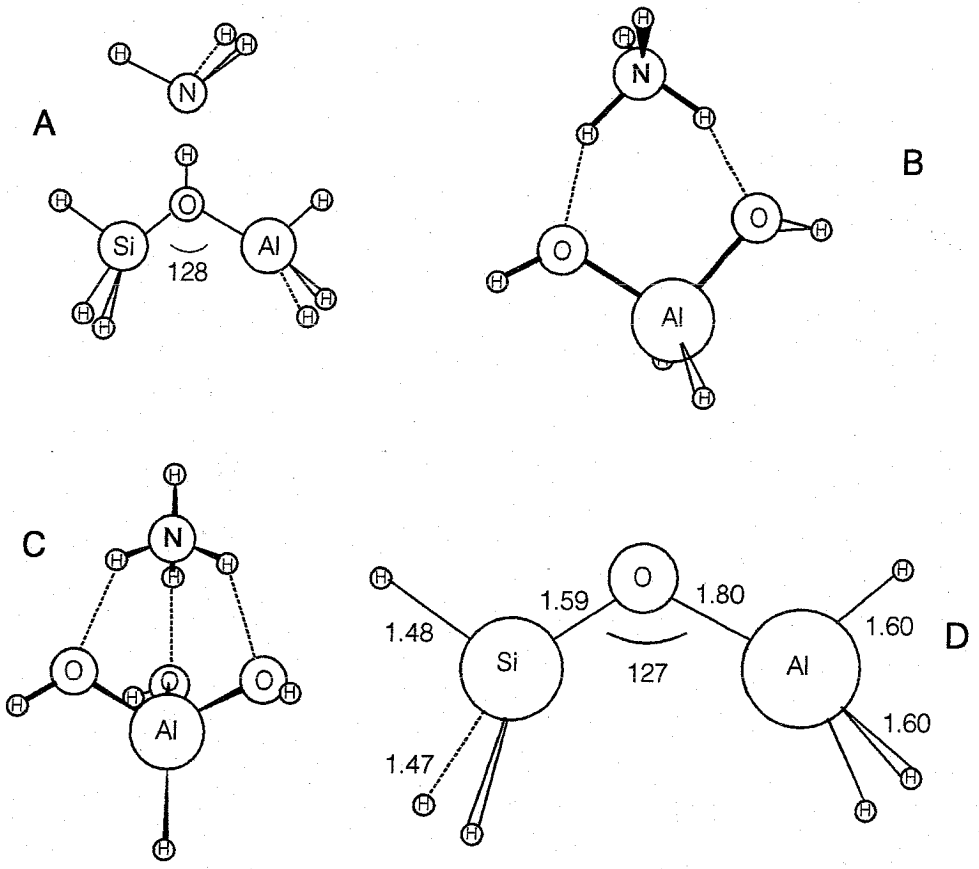

Figure 14. Clusters showing the interaction of NH_3 with the Brønsted site [27].

The equal interaction energies of NH_4^+ coordinated bidentate or tridentate implies that the NH_4^+ ion moves in a very flat potential. Neutron scattering energy loss data show that NH_4^+ is nearly freely rotating in the supercages of the Y-zeolite, but has a slightly more hindered rotation when in the smaller sodalite cage [30].

Whereas in water the basicity of ammonia is larger than that of pyridine, temperature programmed desorption experiments show always a higher temperature of desorption for adsorbed pyridine than ammonia [31,32]. The low basicity of pyridine compared to ammonia in water stems from the high heat of hydration of ammonia compared to pyridine. The gas phase protonation energy of pyridine, however, is 10.8 eV, whereas

Table 2.
The frequencies of the experimental and calculated infrared spectra given in cm^{-1}. Experimental values are for NH_4^+ in: Mordenite (MOR), Faujasite (FAU), Beta (BET) and Erionite (ERI). The other spectra are calculated ones. 2H and 3H are the notation for the doubly and triply bonded NH_4^+. H is the structure in which the proton is attached to the zeolite, the peak given here thus is the OH stretching. COAD is a singly bonded NH_4^+ with one NH_3 coadsorbed (N-H stretching of the proton pointing towards the zeolite is shifted to 2123 cm^{-1}, but is not included in the table because it is mixed with a Si-H stretching).
(I) means that these peaks have a reasonable intensity, the other peaks have negligible intensity but are included for completeness [28]

MOR	FAU	BET	ERI	2H	3H	H	COAD
2780	2800	2970	2840	2623(I)	3103(I)	3142(I)	3153(I)
2930	3040		3068	2740(I)	3141(I)	3360	3363
3180	3270	3200	3260	3418	3478(I)	3478	3401
3400	3360	3460	3384	3495		3483	3473
							3476
							3483

that of NH_3 is 9.9 eV [33]. The difference relates to the higher s-character of the pyridine lone pair compared to that of ammonia. The absence of hydration and the vacuum-type environment of the zeolite is responsible for the stronger basicity of pyridine in the zeolite environment.

Other quantum-chemical cluster calculations on the zeolite proton-polar molecule interaction show similar results.

As discussed in the previous section protonation of H_2O and CH_3OH does not occur. However interaction with the zeolitic proton is very strong and a proton of water and the proton of methanol is strongly interacting with a basic lattice oxygen atom. [24,25]. The ground state is very close to the protonated state. This agrees with the rapid proton-deuterium exchange reaction of deuterated water or methanol with zeolitic protons. The transition-state for the protonation of methanol is sketched in figure 14. Protonated methanol becomes coordinated as bidentate. This can be considered Brønsted acid-Lewis base assisted protonation. The Brønsted acid is the proton, the Lewis base is the other oxygen atom around aluminum to which the methanol proton attaches (figure 15). This can be considered Brønsted acid-Lewis base assisted protonation. The Brønsted acid is the proton, the Lewis base is the other oxygen atom around aluminum to which the methanol proton attaches (figure 14).

These results have an important consequence for the transition state of reactions that proceed via carbenium-ions or carbonium-ion intermediates.

Carbenium-ion formation from ethylene has been studied quantum chemically [35,36]. Ethylene can interact in two ways with the proton. It can form initially a π-complex without proton transfer. In this state interaction is weak. When the proton becomes attached to ethylene (the transition state), the positive charge that develops at the other end of the carbenium-ion becomes stabilized by interaction with the negative charge on another atom around aluminum. This is the Brønsted acid-Lewis base assisted proton

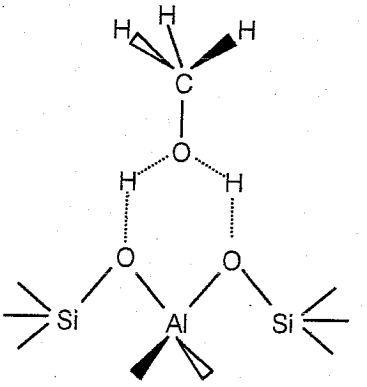

Figure 15. Transition state in the protonation of methanol [34].

transfer mechanism. In the case of ethylene this leads to formation of a stable O-C bond, the σ-complex or surface alkoxide. The formation of σ-complexes has been confirmed by NMR [37,38].

Recently we demonstrated that also for methane, hydrogen-deuterium exchange in a zeolite proceeds by a carbonium-ion state which is not a stable intermediate, but a transition state [39]. The penta-coordinated carbon atom is coordinated bidentate to the two basic oxygen atoms around an $[AlO_4]$ center. The experimentally measured activation energy for proton-deuterium exchange of 120 kJ/mole has such a low value due to the stabilizing zwitter-ionic nature of the carbenium-ion transition state.

7. Concluding remarks

In the previous section the quantum chemistry of the interaction of adsorbates with Brønsted acidic zeolite sites has been discussed. The relative stabilities depend on the deprotonation energy as well as the stabilization of the organic substrate by the negative charge generated on lattice oxygen atoms. The deprotonation energy is sensitive to lattice relaxation and depends on local geometric constraints due to long range structure of the zeolites as well as zeolite composition.

Acid catalysis is controlled by the chemistry of the protonation site as we discussed it here, as well as the interaction of reactant and products molecules with the stabilizing zeolite.

8. References

*. Based in part on: R.A. van Santen, G.J. Kramer, W.P.J.H. Jacobs, In: "Elementary Reaction Steps in Heterogeneous Catalysis", Eds. R.W. Joyner, R.A. van Santen, NATO-ASI 1993, p. 398.

1. G.J. Kramer and R.A. van Santen, J. Am. Chem. Soc, 115 (1993) 2887.
2. J. Sauer and W. Schirmer, In: "Innovation in Zeolite Materials Science (Studies in Surface Science and Catalysis 37), Eds. P.J. Grobet, W.J. Mortier, E.F. Vansant and G. Schulz-Eklhoff, Plenum, New York, 1986, p.323.
3. J. Sauèr, J. Phys. Chem. 91 (1987) 2315.
4. V.B. Kazansky, Acc. Chem. Res. 24 (1991) 379.
5. D. Fenzke, M. Hunger, H. Pfeifer and J. Magn-Reson, 95 (1991) 477.
6. R.A. van Santen, Theoretical Heterogeneous Catalysis, World Scientific (Singapore) 1991, p.204, 320.
7. W.P.J.H. Jacobs, H. Jobic, J.H.M.C. van Wolput and R.A. van Santen, Zeolites 12 (1992) 315.
8. L.M. Kustov, V. Yu. Borovkov and V.B. Kazansky, J. Catal. 72 (1981) 149.
9. J. Sauer, J. Mol. Catal. 54 (1989) 312.
10. H. Jobic, J. Catal. 131 (1991) 289.
11. W.P.J.H. Jacobs, A.J.M. de Man, J.H.M.C. van Wolput and R.A. van Santen, Proceedings, 9th Int. Zeol. Conf., July 5-10, 1992, Montreal;
    W.P.J.H. Jacobs, J.H.M.C. van Wolput, R.A. van Santen, Chem. Phys. Lett. 210 (1993) 32.
12. W.P.J.H. Jacobs, H. Jobic, J.H.M.C. van Wolput and R.A. van Santen, in Zeolites, to appear.
13. R.A. van Santen and D.L. Vogel, Adv. Solid. State Chem. 1 (1989) 151.
14. C.R.A. Catlow and W.C. Mackrodt, Computer Simulations of Solids, Lecture Notes in Physics 66, Springer, Berlin, 1982.
15. G.J. Kramer, N.P. Farragher, B.H.W. van Beest and R.A. van Santen, Phys. Rev. B 43 (1991) 5068.
16. G.J. Kramer, A.J.M. de Man and R.A. van Santen, J. Am. Chem. Soc. 113 (1991) 6435.
17. D. Freude, M. Hunger, H. Pfeifer and W. Schwieger, Chem. Phys. Lett. 128 (1986) 62.
18. U. Lohse, B. Parlitz, V. Parlitz and V. Patzelova, J. Phys. Chem. 93 (1089) 3677.
19. U. Lohse and J. Jänchen, unpubl. results.
20. M. Czjzek, H. Jobic, A.N. Fitch and T. Vogt, J. Phys. Chem. 96 (1992) 1535.
21. K.P. Schröder, J. Sauer, M. Leslie, C.R.A. Catlow and J. Thomas, Chem. Phys. Lett. 188 (1992) 320.
22. M. Peeters, Thesis Eindhoven 1993.
23. A.G. Pelmenchikov, R.A. van Santen, J. Jänchen, E. Meyer, J. Phys. Chem. 97 (1993) 11071.
24. A.G. Pelmenchikov, R.A. van Santen, J.H.M.C. van Wolput, to be published.
25. A.G. Pelmenchikov, R.A. van Santen, J. Phys. Chem. 97 (1993) 10678.
26. E.H. Teunissen, F.B. Duijneveldt and R.A. van Santen, J. Phys. Chem. 96 (1992) 366.
27. E.H. Teunissen, R.A. van Santen, A.P.J. Jansen and F.B. van Duijneveldt, J. Phys. Chem. 97 (1993) 203.

28. E.H. Teunissen, W.P.J.H. Jacobs, A.P.J. Jansen and R.A. van Santen, Proceedings, 9th Int. Zeol. Conf., July 5-10, 1992, Montreal.
29. G.A. Ozin, M.D. Baker, J. Godber and C.J. Gil, J. Phys. Chem. 93 (1989) 2899.
30. W.P.J.H. Jacobs, Thesis Eindhoven 1993.
31. H.G. Karge and V. Dondur, J. Phys. Chem. 94 (1990) 765.
32. H.G. Karge, V. Dondur and J. Weitkamp, J. Phys. Chem. 95 (1991) 283.
33. W.J. Hehre, L. Radow, P.V.R. Schleyer and J.A. Pople, In: "Ab Initio Molecular Orbital Theory", John Wiley & Sohns, (1986).
34. J. Sauer, C. Kölmel, F. Haase and R. Ahlrichs, Proceedings, 9th Int. Zeol. Conf., July 5-10, 1992, Montreal.
35. V.B. Kazansky and I.N. Senchenya, J. Catal. 119 (1989) 108.
36. I.N. Senchenya and V.B. Kazansky, Catal. Lett. 8 (1991) 317.
37. M.T. Aronson, R.J. Gorte, W.E. Farneth and D. White, J. Am. Chem. Soc. 111 (1989) 840
38. J.F. Haw, B.R. Richardson, I.S. Oshiro, N.D. Lazo and J.A. Speed, J. Am. Chem. Soc. 111 (1989) 2052.
39. G.J. Kramer, R.A. van Santen, C.A. Emeis, A.K. Novak, Nature 363 (1993) 529.